Autonomous and portable soft exosuit for hip extension assistance with online walking and running detection algorithm

Jinsoo Kim*, *Student Member, IEEE*, Roman Heimgartner*, Giuk Lee, *Member, IEEE*, Nikos Karavas, David Perry, Danielle Louise Ryan, Asa Eckert-Erdheim, Patrick Murphy, Dabin Kim Choe, Ignacio Galiana, and Conor J. Walsh, *Member, IEEE*

***Abstract*— We present an autonomous and portable hip-only soft exosuit, for augmenting human walking and running that assists hip extension by delivering peak forces of 300N to the user. Different fixed assistance profiles for walking and running were applied based on an online classification algorithm. The approach is based on the biomechanical understanding that the center of mass potential energy fluctuations during walking and running are out of phase. Specifically, we monitor the vertical acceleration with an abdomen-mounted IMU at the moment of maximum hip extension. Validation is demonstrated with six subjects on the treadmill and with eight subjects outdoors. Our results demonstrated a 99.99% accuracy on average over the fourteen participants for various speeds (0.5 – 4m/s), slopes (-10 – 20%), treadmill and overground terrain, loaded (13.6 kg) and unloaded, *Exo On* and *Exo Off* conditions, and different shoe types. Results from an evaluation outdoors overground on the energetics of eight subjects demonstrated a significant reduction for running when comparing *Exo On* to *No Exo* (3.9%) and for walking and running when comparing *Exo On* to *Exo Off* (12.2% and 8.2% respectively). This study represents the first demonstration of an autonomous wearable robot reducing the energy cost of running. Significant variation in response across subjects was observed, highlighting further improvements may be possible via assistance profile individualization with human-in-the-loop optimization.**

I. Introduction

Lower limb wearable exoskeletons have been developed for a wide range of applications, including assisting or augmenting human locomotion and rehabilitation [1-11]. In the field of human performance augmentation in particular, the past decade has seen remarkable breakthroughs in exoskeletons that are able to reduce the metabolic expenditure of walking [3-11].

Initially, tethered devices were the first to achieve a net metabolic reduction during walking. Sawicki *et al.* used artificial pneumatic muscles at ankle joints and showed a statistically significant reduction beyond the level of walking without exoskeleton at 1.75m/s out of several speeds tested [3]. Similarly, Malcolm *et al.* showed a 6% metabolic expenditure reduction using a tethered pneumatic ankle device at 1.38m/s, which is closer to preferred walking speeds [4]. Following the aforementioned work with tethered systems, an ankle exoskeleton came out achieving the first net metabolic reduction with an autonomous system (8%) for subjects walking at 1.5m/s with a 23kg load [5]. After that, there have been a number of wearable robots showing even greater net metabolic reduction during walking. Some of them assisted the ankle joint [8], and the others assisted the hip [9, 10] or both of them [11].

More recently, with the growing interest in augmenting human walking, various groups began to explore how wearable robots can be used to augment human running. Initial pivotal studies that were the first to address this goal highlighted some of challenges and, despite their elegant designs, were not able to demonstrate a reduction in energy cost. Specifically, Elliott *et al.* presented an elastic knee exoskeleton engaged by a clutch and showed an average 27.3% increase in net metabolic cost when running at 3.5m/s compared to running without a device [12]. In another study, Cherry *et al.* developed a pseudo-passive elastic exoskeleton to assist running by adding stiffness in parallel with the entire lower limb, and found an average 58.1% increase in metabolic cost when running with the exoskeleton at 2.3m/s compared to running without it [13].

The results from these past studies can provide us with insights to guide the development of future systems. When considering the design of a wearable robot to assist running, it is clear that minimizing the added mass of the system is critical. While doing so is also important for walking, it is likely more critical for running as the metabolic cost of carrying weight is higher during running than walking [14, 15]. Furthermore, this penalty increases exponentially as the weight becomes more distal, which limits the energy benefit from wearable devices [14-16].

Our group has been developing soft exosuits for augmenting the normal muscle work of healthy individuals [17] as well as restoring function for physically impaired people such as patients poststroke [18, 19]. Exosuits provide particular advantages for assisting human motion as they minimize restrictions to the wearer, do not significantly increase the inertia of limb segments, and eliminate the need to carefully align a robot with biological joints. While much of our work to date has focused on walking [11, 17, 20-28], we believe this approach holds promise to assist with both walking and running. We recently showed that a tethered soft exosuit that assists hip extension could reduce the metabolic cost of running by 5.4% when compared to no suit [29] with a simulation-optimized force profile [30]. Part of the motivation

This material is based upon work supported by the Defense Advanced Research Projects Agency (DARPA), Warrior Web Program (Contract No. W911NF-14-C-0051). This work is also partially funded by the Wyss Institute for Biologically Inspired Engineering and the John A. Paulson School of Engineering and Applied Sciences at Harvard University.

* These authors equally contribute to this work.

J. Kim (e-mail: jinsookim@g.harvard.edu) and C. Walsh (phone: 617-496-7128, e-mail: walsh@seas.harvard.edu) are with the John A. Paulson School of Engineering and Applied Sciences and the Wyss Institute for Biologically Inspired Engineering, Harvard University, Cambridge, MA 02138 USA.

for assisting the hip joint was that, as mentioned previously, there is an increased metabolic penalty when mass is attached distally to a person. Furthermore, a system assisting the hip joint only needs to attach to the waist and upper leg and so can be simplified compared to a full leg system.

From an understanding of the biomechanics of walking and running [31], as well as our past studies [27, 29], it seems likely that different assistive profiles are required for these different activities. Further motivating the fact that walking and running require different assistance strategies is that lower limb muscles show different activation patterns for walking and running [32, 33]. To this end, we need to further develop an online algorithm that detects walking and running accurately and robustly.

Activity classification in general has already been studied extensively, as described in this review paper [34]. Besides, in the field of wearable robotic devices, determination of the user's steady-state activity, as well as the transitions between them, is considered as one of the primary role of the high-level controller [35]. In particular, the latency, accuracy, and number of activities recognized by the classifier must be carefully balanced in order to avoid triggering hazardous or suboptimal control mode changes.

When looking at how to distinguish walking and running gaits, we can consider them from a spatiotemporal, kinematic, biomechanical, or muscular point of view [31-33, 36-38]. A spatiotemporal difference is the duty cycle of stance phase which is greater than 0.5 for walking and less than 0.5 for running. Furthermore, prior studies have shown that at mid-stance, the center of mass (CoM) is highest for walking but lowest for running, meaning that the leg is relatively straight for walking, while the hip, knee and ankle are more flexed during running [31]. In line with this, walking can be modeled as an inverted pendulum, efficiently exchanging potential and kinetic energy out of phase with every step. On the other hand, during running, a mass-spring mechanism causes gravitational potential energy and forward kinetic energy to be in phase [31, 36, 37].

In past work, Parkka *et al.* proposed a decision tree classifier using inertial measurement units (IMUs) on the chest and the wrist to distinguish walking and running [39]. They used the peak frequency of the chest vertical acceleration, which is equivalent to the step frequency, as well as the peak power of the same signal. However, those features do not rely on a strong definition of running, and they show distribution overlap between walking and running, which resulted in an overall classification accuracy of 86%. Two other candidate features, the amplitude of the vertical acceleration at the back [40] and the power spectral entropy of the acceleration at the hip and the dominant wrist [41], were also suggested in another study. However, it was not thoroughly evaluated whether they are discriminative enough in a wide range of speeds, slopes, and anthropometrics of different participants.

In terms of walking and running detection with a wearable robot, Shultz *et al.* designed an algorithm for a knee and ankle prosthesis [42]. They proposed a set of threshold crossing rules which solely rely on shank load, acceleration, and estimated cadence. However, this approach is not suitable for use cases that aim to avoid the use of distally mounted sensors

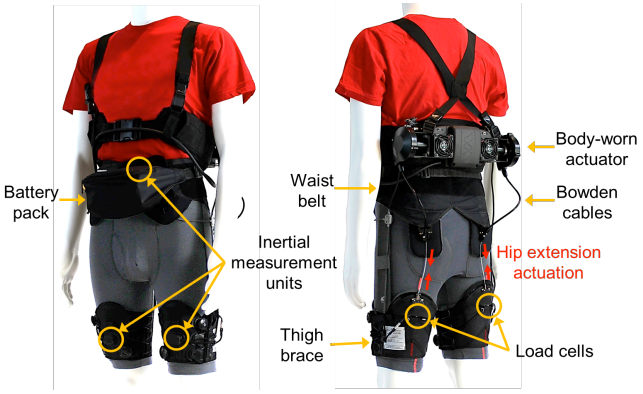

Figure 1. Overview of a hip-only soft exosuit. An actuator and a battery are mounted on the lower back and the bottom part of abdomen, respectively. Two sets of Bowden cables from the actuator are connected to the soft exosuit to provide hip extension assistance.

(e.g. to minimize system complexity). For exoskeletons, a stair ascent and descent detection algorithm was developed using data from sensors at the hip joint and a back-mounted IMU [43], but to date we are not aware of any exoskeletons that classify walking and running gait modes.

In this paper, we present an autonomous and portable hip-only soft exosuit that is able to distinguish between walking and running activities. Our proposed detection algorithm is based on the biomechanical definition that the potential energy during the stance phase of walking is out of phase with that of running. With this algorithm, the user can freely choose to either walk or run at a self-selected gait speed, and the exosuit automatically updates the assistance profile applied by the actuator based on the activity of the wearer. In the following sections, we explain an overview of our hip-only system: suits, actuators, sensors, and control architecture. In addition, we describe the underlying biomechanical aspects of walking and running, introduce the robust and reliable feature used to distinguish between them, and then describe the algorithm in detail. Lastly, we present the accuracy and robustness of the algorithm for many different conditions, and show the performance of our autonomous system by quantifying its impact on wearer energetics during walking and running overground outdoors.

II. System Description

A. Functional apparel components

The front and back views of the hip-only soft exosuit are shown in Figure 1. The overall suit, consisting of a spandex baselayer, a waist belt, two thigh braces, and a battle belt, includes a number of improvements over the previous hip-only exosuit [29, 44]. The apparel components incorporate high-friction materials over specific body areas in the baselayer to help the exosuit stay properly anchored and aligned during walking and running. The waist belt and thigh braces are made of a custom sailcloth material that is lighter than previous materials and eliminates many more layers of textile compared to the previous suit. The thigh brace design has been reduced from multiple sizes to a single adjustable size. This is achieved with a closure system that laces up the thigh and tightens comfortably with a user-friendly dial (L4, Boa Technology Inc., CO, USA). The battle belt is used to mount the actuation unit at the back of the wearer and has been

modified from a commercial product (VC-Time Tactical Belt, VC-Time, USA).

Three IMUs (MTi-3 AHRS, Xsens Technologies B.V., Enschede, Netherlands) are mounted on the abdomen and the anterior part of each thigh. The IMU on the abdomen measures CoM acceleration in the global frame to distinguish walking and running gaits. The two IMUs on the thighs measure the thigh segment angle to detect maximum hip flexion (MHF) and maximum hip extension (MHE) gait events.

B. *Actuation unit*

As shown in Figure 1, a two-degree of freedom (DoF) actuation unit is mounted at the wearer's back, and the anchoring points of the Bowden cables are at the bottom left and right of the waist belt as well as at the middle center of the thigh braces from the posterior view. The motors deliver active assistance by retracting the inner Bowden cable that then generates an assistive torque at the hip joint. Two load cells (LSB200, FUTEK Advanced Sensor Technology, Inc., CA, USA) are integrated into the anchoring point of each thigh brace to measure the cable force.

Each DoF consists of an electronically commutated 4-pole power motor (#305013, Maxon, Switzerland) that is connected to a gearbox of ratio 51:1 (#326664, Maxon, Switzerland) and drives a 40-mm radius multi-wrap pulley. An incremental encoder (#225778, Maxon, Switzerland) that has 2000 pulses per revolution is mounted on the motor to measure the motor position. A servomotor driver (Gold Twitter, Elmo Motion Control Ltd., Israel) integrated into a custom electronic board controls each motor in a closed loop. A removable battery consisting of two 6-cell Li-Po units (3.7Ah) is placed on the abdomen and it lasts approximately 7.5 km with a peak force of 300N. The overall system weight is 4.7 kg including 2.6 kg of the actuation unit, 1.1 kg of suit components and sensors, and 1.0 kg of battery.

C. *Control system architecture*

The goal of the controller is to deliver hip extension force in synchrony with human gait dynamics. An IMU-based iterative algorithm detects MHF by tracking the sign change in angular velocity from the thigh IMU and estimates the wearer's phase in the gait cycle based on that gait event [28]. A force-based position controller is used to create the hip extension force profile with desired onset, peak, and end timings. This iterative controller adjusts the timing and magnitude of the motor position profile on a step-by-step basis to consistently deliver the assistive force profile despite variability in the wearer's gait or migration of suit components [28].

An Atmel 32-bit microcontroller unit (MCU) (ATSAME70N21, Atmel Corporation, CA, USA) is used to perform high-level controller calculations at 1kHz, to communicate with the motor controllers, sensors, host laptop, and to save high-frequency system data on an SD card. The 8-bit microprocessor units (PIC18F25K80, Microchip Technology Inc., AZ, US) attached to each IMU are used to read analog force signals from the load cell as well as kinematic information (Euler angles, angular velocities, accelerations) for all three axes from the IMU via a universal asynchronous receiver/transmitter (UART). In order to get a drift-free orientation estimate, each IMU is equipped with a built-in sensor fusion algorithm based on extended Kalman filter. The controller area network (CAN) communication protocol is used for communication between the 8-bit MCUs, motor controllers, and the 32-bit MCU. In addition, the 32-bit MCU communicates with the host laptop via a Bluetooth module (BT900-SC, Laird Technologies, UK) at 100 Hz for real-time data visualization, while simultaneously saving system data in the onboard SD card (SDSQUNC-032G-AN6IA, Sandisk, CA, US) at 1 kHz.

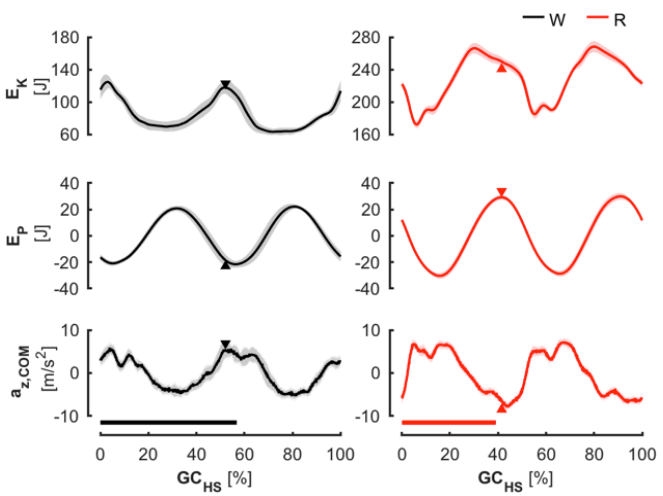

Figure 2. Forward kinetic energy (E_k), gravitational potential energy (E_p), and the CoM vertical acceleration ($a_{z,CoM}$) of a representative participant during walking at 1.5 m/s (left/black) and running at 2.5 m/s (right/red) measured by a motion capture system (Vicon, Oxford, UK) in our previous study [46]. E_k and E_p are calculated based on the horizontal velocity and the vertical position of the motion capture markers at the left and right iliac crests. The solid lines and shaded light regions represent the average and the standard deviation of ten strides, respectively. The horizontal axis is the gait cycle segmentation based on heel strike ($\equiv GC_{HS}$) by measuring the ground reaction forces from an instrumented treadmill (Bertec, OH, USA). The black and red bars on the gait cycle axis represent the stance phase of the right leg, and the remaining portion corresponds to swing phase of the same leg. Maximum hip extension (MHE) is marked as a triangle.

III. Online Walking and Running Detection Algorithm

A. *Biomechanical differences between walking and running*

During human locomotion, the forward kinetic energy (E_k) of the center of mass (CoM) oscillates similarly as a function of the gait cycle for walking and running, as it is minimal at the mid-stance for both gait modes [31, 37]. However, the potential energy (E_p) of the CoM fluctuates differently: at mid-stance, it is maximal for walking (i.e. out of phase with kinetic energy) and minimal for running (i.e. in phase with kinetic energy) as shown in Figure 2, which implies that E_p could be used as a feature to distinguish between walking and running activities.

The potential energy is calculated by the following equation

$$E_p = mgh_{CoM}, \tag{1}$$

where m, g, and h_{CoM} are the mass, the gravitational acceleration, and the CoM height, respectively. Because m and g are constant, the potential energy is directly proportional to

h_{CoM}, which means that h_{CoM} can be used as a feature instead of E_p to distinguish walking and running. Unfortunately, it is challenging to estimate h_{CoM} reliably and accurately for an extended period of time using body-worn sensors because of drift-inducing estimation errors [45]. Instead, the CoM vertical acceleration, $a_{z,CoM}$, can be extracted relatively easily using an IMU. Furthermore, since $a_{z,CoM}$ and h_{CoM} are strongly related to each other as follows

$$a_{z,CoM} = \frac{d^2 h_{CoM}}{dt^2}, \quad (2)$$

$a_{z,CoM}$ during the stance phase should also show a contrasting trend between walking and running.

First, we explored the feasibility of using the $a_{z,CoM}$ signal to differentiate between walking and running using motion capture data collected as part of a prior study [46]. As we speculated in the previous section, $a_{z,CoM}$ had a clearly different profile for the stance phases of walking and running: at mid-stance, it is minimal for walking and it is maximal for running, as illustrated in Figure 2. Note that the stance phase portion occurs approximately from 0% to 60% for walking and from 0% to 40% for running.

An additional challenge was to leverage sensors in the system to be able to estimate this difference in $a_{z,CoM}$. Indeed, the stance phase (i.e. heel-strike) cannot be detected accurately and robustly using only body-worn sensors above the knee joint, which means that it is difficult for the controller to detect the mid-stance timing. Thus, another gait event that is able to catch the contrasting aspect of $a_{z,CoM}$ is needed. As shown in Figure 2, maximum hip extension (MHE), marked as triangles, coincide with a minimum and maximum in E_p for walking and running, respectively. In addition, the corresponding $a_{z,CoM}$ at MHE (which is close enough to toe-off timing for both walking and running, as shown in Figure 2) is positive for walking and negative for running.

B. Feature selection – The global frame vertical acceleration of the abdomen IMU at MHE

Our team has previous experience in detecting gait events using IMUs [28]. Since the MHE can be reliably extracted using thigh IMUs, we propose that using IMUs mounted on the abdomen and both thighs can extract the feature of interest.

First of all, the CoM vertical acceleration ($a_{z,CoM}$) can be approximated by the vertical acceleration of the abdomen IMU ($a_{z,abd.}$), as shown in Figure 3. To compute this, the global frame (East-North-Up) abdomen acceleration was computed from the local frame (i.e. body-attached sensor frame) acceleration by the following equation

$$\begin{pmatrix} a_{x,abd.} \\ a_{y,abd.} \\ a_{z,abd.} + g \end{pmatrix} = R_z(\psi) R_y(\theta) R_x(\phi) \cdot \vec{a}_{abd.local}. \quad (3)$$

where $a_{x,abd.}$, $a_{y,abd.}$, $a_{z,abd.}$ are the x-, y-, and z-components of the global frame acceleration of the abdomen IMU. Here, the z-direction is parallel to gravity. ϕ, θ, and ψ are the three Euler angles of the abdomen IMU: roll, pitch, and yaw angles, respectively. $R_x(\phi)$, $R_y(\theta)$, and $R_z(\psi)$ are the rotation matrices with respect to the x-, y-, and z-axis, respectively. $\vec{a}_{abd.local}$ is the abdomen IMU acceleration in the local frame.

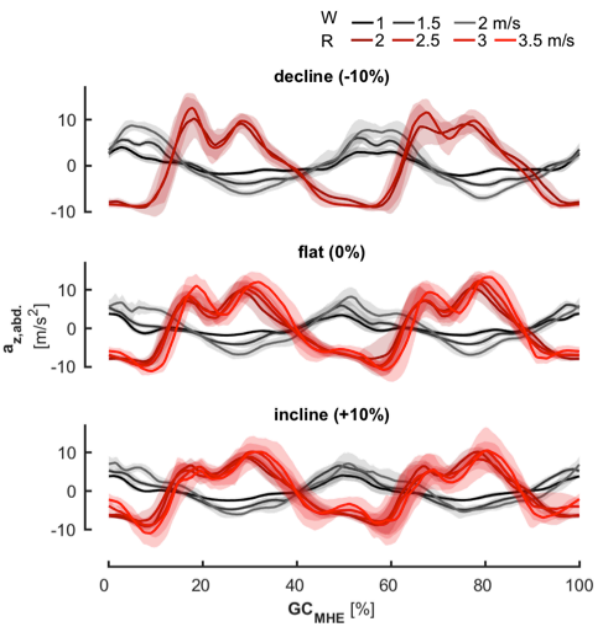

Figure 3. Global frame vertical acceleration of the abdomen IMU ($a_{z,abd.}$) of a representative participant walking and running on treadmill at various slopes and speeds. The black-hued plots are for walking, and the red-hued plots are for running. The gait cycle is segmented based on MHE (≡GC_{MHE}) using the angular velocity of thigh IMU. Thus, the value at 0% corresponds to the abdomen feature. The 2 m/s speed condition is included in both walking and running, because it is close to the walk-to-run transition speed.

Based on motion capture data analysis in Section III. A, we selected our feature as the global frame vertical acceleration of the abdomen IMU ($a_{z,abd}$) at MHE, which is called the abdomen feature (f_A). We further validated the robustness of this abdomen feature for different slopes and speeds. In Figure 3, the global frame vertical acceleration of the abdomen IMU ($a_{z,abd.}$) is shown for a representative participant. Signals were segmented based on MHE of the right leg, which corresponds to 0% on the x-axis. Even though small variations in the timing of the MHE were observed (e.g. walking downslope or running upslope exhibiting feature values closer to 0), the abdomen feature was found to be robust enough from a biomechanical point of view.

C. Implementation of online detection algorithm

An online walking and running detection algorithm is implemented on top of the force-based position controller according to the structure shown in Figure 4. As mentioned in Section III. B, the abdomen vertical acceleration at MHE (f_A) is used as a distinctive feature between the two gait modes. Using this, a heuristic rule-based classifier relies on thresholding of this feature to classify each step as either walking or running gait, and combines the independent outputs obtained from each leg. The system will switch its gait mode and corresponding assistance profile to the other only if the walking/running flags from both legs are changed. A unique rule, using 0 m/s^2 as a threshold, could be used given the biomechanical definition of the feature, but a small tolerance margin – that is the same for all subjects – is implemented to increase reliability.

Note that supplementary conditions on the acceleration signal are verified in the heuristic rule-based classifier to increase robustness for various slope and speed conditions as

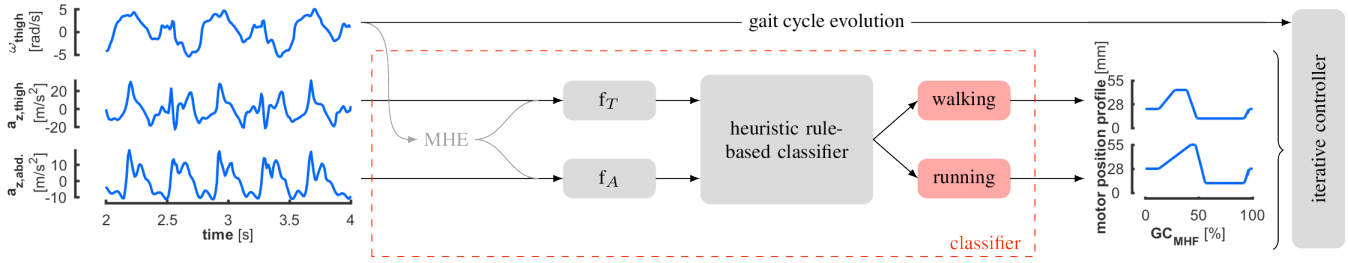

Figure 4. Controller algorithm outline depicting the classification of gait modes. Starting from a thigh and abdomen IMU signals as inputs, features (f_T – thigh feature, f_A – abdomen feature) residing in the vertical acceleration, which is based on the dynamic definition of walking and running, are extracted and a heuristic rule-based classifier distinguishes walking and running gaits. The classifier output is then used to switch assistance profiles. The step-by-step motor position profile is updated when MHF is detected, as described in [28]. The gait cycle is segmented based on MHF (≡GC_{MHF}).

well as for inter-subject variability in gait kinematics: To avoid spurious and frequent switching of the gait mode flag, the algorithm checks that the feature is above (or below for walk-to-run transition) a given threshold for at least two consecutive steps before triggering a run-to-walk transition. However, when the feature value goes from a strongly positive to strongly negative value, or vice-versa, the controller allows a faster one step based transition. In this case, the thigh vertical acceleration ($a_{z,thigh}$) at MHE, called the thigh feature (f_T), is additionally checked in a similar way to confirm the fast transition. This strategy allowed the algorithm to be sensitive enough to prevent uncomfortable situations when transiting between locomotion modes, but ensured an increased robustness during steady-state locomotion.

D. *Walking and running profile switching controller*

At the end of each step, motor position amplitudes are stored separately for walking and running modes. When a transition is detected, the high-level controller retrieves the memorized position level previously recorded from the last three steps corresponding to the new gait mode and updates the current motor position command based on this, allowing for fast transitioning of profiles.

IV. Human Subject Experiments

Two types of human subject experiments were conducted. First, we evaluated the detection algorithm during treadmill tests. After ensuring the accuracy of the algorithm, overground tests were conducted to validate the robustness in a real-world environment. In addition, the energy expenditure of participants was collected to determine the metabolic effects of the soft exosuit.

A. *Treadmill tests*

The walking and running detection algorithm was evaluated for six participants (28 ± 2 years old; 176.5 ± 8.5 cm; 76.0 ± 12.9 kg) walking at three different speeds (1, 1.5 and 2 m/s) and running at four different speeds (2, 2.5, 3 and 3.5 m/s) on a treadmill (PPS MED, Woodway, WI, USA) for various inclines (-10, -5, 0, 5, 10, 15 and 20 %). For decline conditions, the testing speed was limited to 2.5 m/s due to treadmill specifications. For all conditions, the system was worn but not actuated. Apart from its weight, no additional load was carried, and the participants wore their own comfortable sneakers. In order to confirm the robustness of the algorithm for even extreme cases, a randomly selected participant tried a loaded condition (13.6 kg) while wearing military boots for all the aforementioned condition with

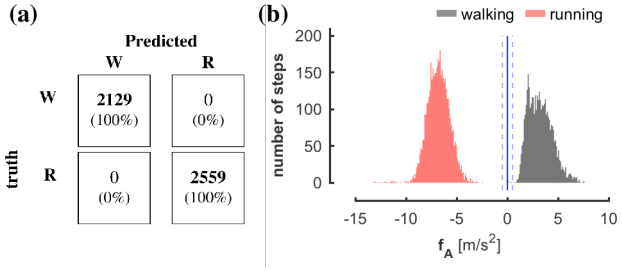

Figure 5. The performance of proposed detection algorithm for all the participant, speed, and slope conditions during treadmill tests. (a) Confusion matrix for the detection algorithm accuracy. The rows are the ground truth and the columns are the predicted result output by the proposed algorithm. The off-diagonal elements in this matrix are detection errors. (b) Abdomen feature (f_A) distributions. The red histogram bar represents the ground truth of running and the black ones are the ground truth of walking. The feature shows negative value for running and positive for walking. The blue solid line is a theoretical boundary (= 0 m/s^2), and dotted line represents a small tolerance margin for thresholds allowing increased robustness.

additional 0.5m/s walking and 4.0m/s running conditions. For each slope condition, the participant stepped onto the treadmill, walked or ran for 40 steps, stepped off and the speed condition was changed. IMU signals and algorithm output were streamed at 100 Hz from the system to a host laptop via Bluetooth. For each trial, the first three steps recorded were discarded due to the short transition periods between rest and locomotion at certain speeds.

The algorithm was able to differentiate walking and running perfectly for all the conditions even given the variability in the participants, locomotion speeds, and slopes. Indeed, the full detection algorithm combining both features with the classification rules mentioned before perfectly predicted the actual locomotion modes for each stride, as shown by the confusion matrix in Figure 5(a).

This can be explained by looking at the distribution of the abdomen feature shown in Figure 5(b). Specifically, the distributions for walking and running do not overlap at all, which indicates reliability and robustness of such a distinctive feature. The mean and standard deviations of the abdomen feature are 3.23 ± 1.19 m/s^2 (walking) and -6.82 ± 1.12 m/s^2 (running), respectively.

B. *Overground tests*

As shown in Figure 6, an overground pilot test was performed with eight participants (28 ± 3 years old; 181.0 ± 7.9 cm; 78.4 ± 9.0 kg) to evaluate the performance of the detection algorithm and human metabolic responses during

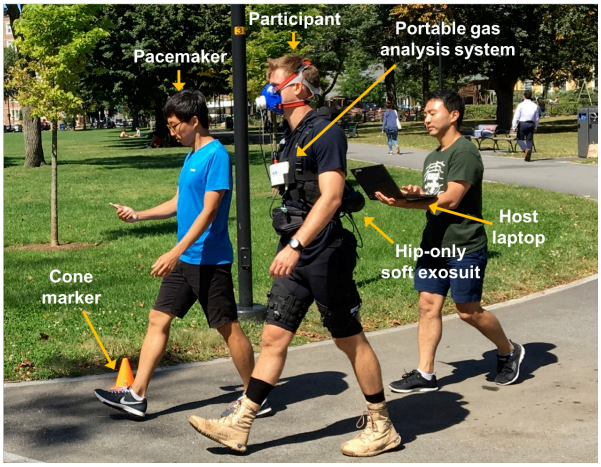

Figure 6. The overview of the outdoor test setup. The participant wore the hip-only soft exosuit. The pacemaker guided the participant while checking the elapsed time between the cone markers in order to maintain the gait speed as specified in the protocol. The metabolic cost was assessed by indirect calorimetry using a portable gas analysis system. The system data of the hip-only soft exosuit was recorded and visualized with a host laptop via Bluetooth communication.

walking and running. All participants reported no history of musculoskeletal injuries or other musculoskeletal diseases and provided written informed consent prior to participating in the study. The study was approved by the Harvard Medical School Committee on Human Studies.

The protocol consisted of three trials: one without wearing the device (*No Exo*), another with the soft exosuit unpowered (*Exo Off*), and one powered with the actuator providing a peak cable force of 300 N, which corresponds to a peak moment of 0.37 Nm kg^{-1} (*Exo On*). Each trial consisted of a 2.2 km course with four laps of 550m. The participants completed the first lap by walking at 1.5m/s, the next two laps by running at 2.5m/s, and the last lap by walking again at 1.5 m/s. Five cone markers were placed every 110m and a pacemaker monitored the walking speed with a stop watch to maintain a constant gait speed. The order of trials was randomized across participants and a minimum ten-minute rest was taken between the trials to prevent any fatigue effects.

In order to evaluate the robustness of the detection algorithm, a research team member carrying the control laptop manually marked a controller flag when a walk-to-run or run-to-walk transition was observed in the participant's gait. This was used as the ground truth signal for evaluation. The timings of those marks were later corroborated by looking at step frequency during post processing of the data. The one step before and after the ground truth of gait mode change were labeled as transition periods.

The typical evolution over time of the abdomen feature and the detection algorithm output are reported together with the ground truth in Figure 7(a) for a single representative participant. The full algorithm accuracy is reported in Figure 7(b) for the eight participants' *Exo On* trial. To illustrate the detection algorithm performance, the feature distribution for the current and previous step from both legs taken separately is shown in Figure 7(c).

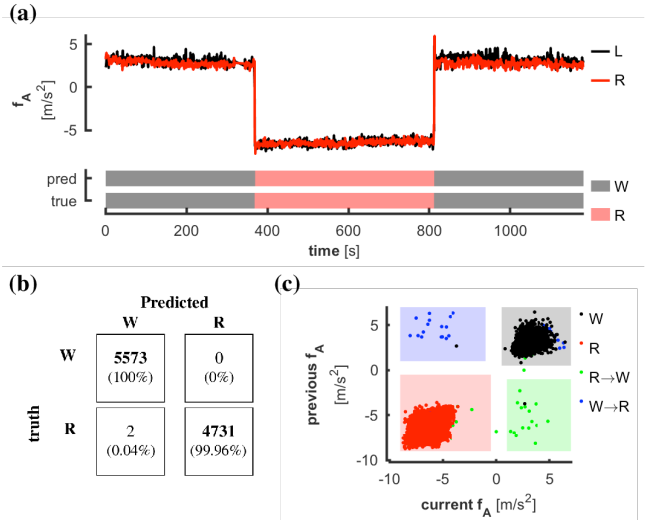

Figure 7. Performance of the proposed detection algorithm for all the participants' *Exo On* trial during overground tests. (a) Typical evolution of the abdomen feature (f_A) over time (left MHE based: black, right MHE based: red), as well as the detection algorithm output (upper horizontal bar) and ground truth (lower horizontal bar) for one representative participant. (b) Confusion matrix for the detection algorithm accuracy. (c) The abdomen feature (f_A) distribution for the current and previous steps together with the classifier decision rules. The color of each data point indicates the ground truth (walking: black, running: red, run-to-walk: green, walk-to-run: blue). The shaded light rectangular regions represent the within threshold boundary set in the heuristic rule-based classifier (black and green: walking, red and blue: running). If the feature is plotted in the white region, the classifier maintains the previously determined gait mode.

The detection algorithm accuracy was 100 % for walking and 99.96 % for running, as shown in Figure 7(b). Note that the only two steps that were incorrectly classified occurred immediately after walking to running transitions, indicating a slightly longer transition delay, but no robustness issue. Figure 7(c) shows how transition steps are identified correctly from the abdomen feature changing from strongly positive to strongly negative values for walk-to-run transitions, and vice versa for run-to-walk transitions, in only one step. During steady-state locomotion, the feature always lies within the boundaries defined by the classifier (i.e. black region for walking and red region for running).

Metabolic cost was assessed using indirect calorimetry with a portable gas analysis system (K4b2, Cosmed, Roma, Italy), which enabled the measurement of expired gas concentrations and volumes. Carbon dioxide and oxygen rates were used to calculate metabolic power with the Brockway equation [47]. Net metabolic power was obtained by subtracting the metabolic power obtained during a standing trial performed at beginning of the *No Exo* trial from the metabolic power of each trial (*No Exo*, *Exo Off*, and *Exo On*). The metabolic power for walking and running were obtained by averaging the last two minutes of the first and last laps, and the last two minutes of the third lap, respectively, to get steady-state value during each gait mode.

During walking, *Exo On* reduced the metabolic cost of walking with respect to *No Exo* and *Exo Off* and by 2.7% (range -12.3 to 24.4%) and 12.2% (range 3.4 to 32.7%), respectively with a negative value representing an increase in metabolic cost in some cases. During running, *Exo On*

reduced the metabolic cost of running with respect to *No Exo* and *Exo Off* by 3.9% (range -1.1 to 8.4%) and 8.2% (range 1.3 to 15.6%). The net metabolic power of walking and running for each trial are reported in Figure 8 and Table I.

V. Discussion and Conclusion

This study represents the first demonstration of an autonomous wearable robot reducing the energy cost of running overground. The net metabolic reduction for running was pretty consistent across the all eight subjects, and the *Exo On* condition showed a statistically significant reduction compared to both *No Exo* and *Exo Off* trials. Previously, our group achieved 5.4% (9.1%) metabolic reduction for running on a treadmill at 2.5m/s with a tethered soft exosuit compared to *No Exo (Exo Off)* [29]. Considering that this study was with an autonomous soft exosuit, the 3.9% reduction we found for running is somewhat expected due to the metabolic penalty associated with the system weight.

Another contribution of this paper is that the system is able to differentiate between walking and running, delivering a different fixed assistance profile for each gait. Our gait classification algorithm showed a 99.99% accuracy on average over fourteen participants on the treadmill and overground, and was robust to various speeds (0.5 – 4m/s), slopes (-10 – 20%), treadmill and overground, loaded (13.6 kg) and unloaded, *Exo On* and *Exo off* conditions, and different shoe types (military boots and sneakers).

A surprising finding from this study was that the net metabolic reduction for walking showed very high inter-subject variability. Some subjects got a relatively large metabolic reduction (24.4%) during the *Exo On* trial compared to *No Exo* condition, but others showed a negative metabolic reduction, increase in energy expenditure (-12.3%). Given that the same fixed profile [27] of assistance was given to all subjects, our findings in this study motivate applying human-in-the-loop optimization methods to individualize assistance profiles [48-50]. Using a Bayesian Optimization and a human-in-the-loop approach, our group has previously demonstrated low variability and high metabolic reduction (17.4±3.2%) for treadmill walking when comparing normal walking to assistance with a tethered version of the soft exosuit presented here [50].

Acknowledgment

The authors would like to thank Maria Athanassiu, Brice Mikala Iwangou, Nicolas Menard, Dorothy Orzel, Taylor Greenberg Goldy, Lauren Baker, Ye Ding, and Sarah Sullivan for their contribution to this work. J. Kim also appreciates the financial support from the Samsung Scholarship.

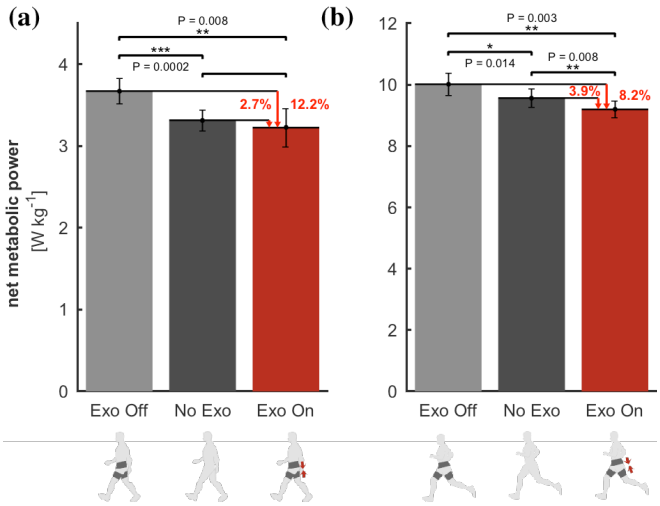

Figure 8. Net metabolic power during an overground test for (a) walking at 1.5m/s and (b) running at 2.5m/s. Solid bars indicate inter-subject mean of net metabolic power, while error bars indicate standard error of the mean (SEM). The grey, black, and red bars are *Exo Off*, *No Exo*, and *Exo O*n trials, respectively. Repeated measures analysis of variance (ANOVA) was conducted across three conditions to verify the effect of hip extension assistance on metabolic cost, with significance set as $P < 0.05$.

TABLE I. NET METABOLIC POWER (MEAN ± SEM)

	Exo Off	***No Exo***	***Exo On***
Walking	3.67 ± 0.15	3.32 ± 0.13	3.23 ± 0.23
Running	10.02 ± 0.37	9.56 ± 0.30	9.20 ± 0.28

References

[1] R. Riener, L. Lünenburger, S. Jezernik, M. Anderschitz, G. Colombo, and V. Dietz, "Patient-cooperative strategies for robot-aided treadmill training: First experimental results," *IEEE Trans. Neural Syst. Rehabil. Eng.*, vol. 13, no. 3, pp. 380–394, 2005.

[2] H. Herr, "Exoskeletons and orthoses: classification, design challenges and future directions," *J. Neuroeng. Rehabil.*, vol. 6, p. 21, 2009.

[3] G. S. Sawicki and D. P. Ferris, "Powered ankle exoskeletons reveal the metabolic cost of plantar flexor mechanical work during walking with longer steps at constant step frequency," *J. Exp. Biol.*, vol. 212, no. 1, pp. 21–31, 2009.

[4] P. Malcolm, W. Derave, S. Galle, and D. De Clercq, "A simple exoskeleton that assists plantarflexion can reduce the metabolic cost of human walking," *PLoS One*, vol. 8, no. 2, e56137, 2013.

[5] L. M. Mooney, E. J. Rouse, and H. M. Herr, "Autonomous exoskeleton reduces metabolic cost of walking," *J. Neuroeng. Rehabil.*, vol. 11, p. 151, 2014.

[6] S. H. Collins, M. B. Wiggin, and G. S. Sawicki, "Reducing the energy cost of human walking using an unpowered exoskeleton," *Nature*, vol. 522, no. 7555, pp. 212–215, 2015.

[7] R. W. Jackson and S. H. Collins, "An experimental comparison of the relative benefits of work and torque assistance in ankle exoskeletons," *J. Appl. Physiol.*, pp. 541–557, 2015.

[8] L. M. Mooney and H. M. Herr, "Biomechanical walking mechanisms underlying the metabolic reduction caused by an autonomous exoskeleton," *J. Neuroeng. Rehabil.*, vol. 13, no. 4, pp. 1–12, 2016.

[9] K. Seo, J. Lee, Y. Lee, T. Ha, and Y. Shim, "Fully autonomous hip exoskeleton saves metabolic cost of walking," in *Proc. IEEE Int. Conf. Robot. Autom. (ICRA)*, pp. 4628–4635, Jun, 2016.

[10] J. Lee, K. Seo, B. Lim, J. Jang, K. Kim, and H. Choi, "Effects of assistance timing on metabolic cost, assistance power, and gait parameters for a hip-type exoskeleton," in *Proc. IEEE Int. Conf. Rehabil. Robot (ICORR)*, pp. 498–504, 2017.

[11] B. T. Quinlivan, S. Lee, P. Malcolm, D. Rossi, M. Grimmer, C. Siviy, N. Karavas, D. Wagner, A. Asbeck, I. Galiana, and C. J. Walsh, "Assistance magnitude versus metabolic cost reductions for a tethered multiarticular soft exosuit," *Sci. Robot.*, vol. 2, no. 2, eaah4416, 2017.

[12] G. Elliott, G. S. Sawicki, A. Marecki, and H. Herr, "The biomechanics and energetics of human running using an elastic knee exoskeleton," in *Proc. IEEE Int. Conf. Rehabil. Robot. (ICORR)*, Jun, 2013.

[13] M. S. Cherry, S. Kota, A. Young, and D. P. Ferris, "Running with an elastic lower limb exoskeleton," *J. Appl. Biomech.*, vol. 32, no. 3, pp. 269–277, 2016.

[14] Y. Epstein, L. A. Stroschein, and K. B. Pandolf, "Predicting metabolic cost of running with and without backpack loads," *Eur. J. Appl. Physiol. Occup. Physiol.*, vol. 56, no. 5, pp. 495–500, 1987.

[15] S. Sovero, N. Talele, C. Smith, N. Cox, T. Swift, and K. Byl, "Initial Data and Theory for a High Specific-Power Ankle Exoskeleton Device," *in Proc. Int. Sym. Exp. Robot.*, pp. 355-364, Oct, 2016.

[16] J. R. Franz, C. M. Wierzbinski, and R. Kram, "Metabolic cost of running barefoot versus shod: Is lighter better?," *Med. Sci. Sports Exerc.*, vol. 44, no. 8, pp. 1519–1525, 2012.

[17] F. A. Panizzolo et al., "A biologically-inspired multi-joint soft exosuit that can reduce the energy cost of loaded walking," *J. Neuroeng. Rehabil.*, vol. 13, no. 1, p. 43, 2016.

[18] L. N. Awad. J. Bae, K. O'Donnell, S. M. M. De Rossi, K. Hendron, L. H. Sloot, P. Kudzia, S. Allen, K. G. Holt, T. D. Ellis, and C. J. Walsh, "A soft robotic exosuit improves walking after stroke," *Sci. Transl. Med*., vol. 9, eaai9084, 2017.

[19] J. Bae, S. M. M. De Rossi, K. O'Donnell, K. L. Hendron, L. N. Awad, T. R. T. Dos Santos, V. L. De Araujo, Y. Ding, K. G. Holt, T. D. Ellis, and C. J. Walsh, "A soft exosuit for patients with stroke: Feasibility study with a mobile off-board actuation unit," in *Proc. IEEE Int. Conf. Rehabil. Robot. (ICORR)*, pp. 131–138, Aug, 2015.

[20] A. T. Asbeck, R. J. Dyer, A. F. Larusson, and C. J. Walsh, "Biologically-inspired soft exosuit," in *Proc. IEEE Int. Conf. Rehabil. Robot. (ICORR)*, Jun, 2013.

[21] M. Wehner, B. Quinlivan, P. M. Aubin, E. M-. Villalpando, M. Baumann, L. Stirling, K. Holt, R. Wood, and C. Walsh, "A lightweight soft exosuit for gait assistance," in *Proc. IEEE Int. Conf. Robot. Autom. (ICRA)*, pp. 3362–3369, May, 2013.

[22] Y.-L. Park, B. Chen, N. O. Perez-Arancibia, D. Young, L. Stirling, R. J. Wood, E. Goldfield, and R. Nagpal, "Design and control of a bio-inspired soft wearable robotic device for ankle-foot rehabilitation," *Bioinspiration & Biomimetics*, vol. 9, no. 1, 016007, 2014.

[23] Y.-L. Park, J. Santos, K. G. Galloway, E. C. Goldfield, and R. J. Wood, "A soft wearable robotic device for active knee motions using flat pneumatic artificial muscles", in *Proc. IEEE Int. Conf. Robot. Autom. (ICRA)*, pp. 4805–4810, Aug, 2014.

[24] A. T. Asbeck, K. Schmidt, and C. J. Walsh, "Soft exosuit for hip assistance," *Rob. Auton. Syst.*, vol. 73, pp. 102–110, 2015.

[25] A. T. Asbeck, S. M. M. De Rossi, K. G. Holt, and C. J. Walsh, "A biologically inspired soft exosuit for walking assistance," *Int. J. Rob. Res.*, vol. 34, no. 6, pp. 744–762, 2015.

[26] V. Bartenbach, K. Schmidt, M. Naef, D. Wyss, and R. Riener, "Concept of a soft exosuit for the support of leg function in rehabilitation," in *Proc. IEEE Int. Conf. Rehabil. Robot. (ICORR)*, pp. 125–130, Aug, 2015.

[27] Y. Ding, F. A. Panizzolo, C. J. Siviy, P. Malcolm, I. Galiana, K. G. Holt, and C. J. Walsh, "Effect of timing of hip extension assistance during loaded walking with a soft exosuit," *J. Neuroeng. Rehabil.*, vol. 13, no. 87, 2016.

[28] Y. Ding, I. Galiana, C. Siviy, F. A. Panizzolo, and C. Walsh, "IMU-based iterative control for hip extension assistance with a soft exosuit," in *Proc. IEEE Int. Conf. Robot. Autom. (ICRA)*, pp. 3501–3508, Jun, 2016.

[29] G. Lee, J. Kim, F. A. Panizzolo, Y. M. Zhou, L. M. Baker, I. Galiana, P. Malcolm, and C. J. Walsh, "Reducing the metabolic cost of running with a tethered soft exosuit," *Sci. Robot.*, vol. 2, no. 6, eaan6708, 2017.

[30] T. K. Uchida, A. Seth, S. Pouya, C. L. Dembia, J. L. Hicks, and S. L. Delp, "Simulating Ideal Assistive Devices to Reduce the Metabolic Cost of Running," *PLoS One*, vol. 11, no. 9, p. e0163417, 2016.

[31] D. M. Bramble and D. E. Lieberman, "Endurance running and the evolution of Homo," *Nature*, vol. 432, no. 7015, pp. 345–352, 2004.

[32] E. Arnold, S. Hamner, A. Seth, M. Millard, and S. Delp, "How muscle fiber lengths and velocities affect muscle force generation as humans walk and run at different speeds," *J. Exp. Biol.*, vol. 216, pp. 2150-60, 2013.

[33] B. I. Prilutsky and R. J. Gregor, "Swing- and support-related muscle actions differentially trigger human walk-run and run-walk transitions," *J. Exp. Biol.*, vol. 204, no. 13, pp. 2277–2287, 2001.

[34] S. J. Preece, J. Y. Goulermas, L. P. J. Kenney, D. Howard, K. Meijer, and R. Crompton, "Activity identification using body-mounted sensors—a review of classification techniques," *Physiol. Meas.*, vol. 30, no. 4, pp. 1–33, 2009.

[35] M. R. Tucker et al., "Control strategies for active lower extremity prosthetics and orthotics: a review," *J. Neuroeng. Rehabil.*, vol. 12, no. 1, 2015.

[36] G. A. Cavagna, H. Thys, and A. Zamboni, "The sources of external work in level walking and running," *J. Physiol.*, vol. 262, no. 3, pp. 639–657, 1976.

[37] C. T. Farley and D. P. Ferris, "Biomechanics of walking and running: center of mass movements to muscle action," *Exerc Sport Sci Rev*, vol. 26, pp. 253–285, 1998.

[38] D. J. Farris and G. S. Sawicki, "The mechanics and energetics of human walking and running: a joint level perspective," *J. R. Soc. Interface*, vol. 9, no. 66, pp. 110–118, 2012.

[39] J. Pärkkä, M. Ermes, P. Korpipää, J. Mäntyjärvi, J. Peltola, and I. Korhonen, "Activity classification using realistic data from wearable sensors.," *IEEE Trans. Inf. Technol. Biomed.*, vol. 10, no. 1, pp. 119–128, 2006.

[40] S. H. Lee, H. D. Park, S. Y. Hong, K. J. Lee, and Y. H. Kim, "A study on the activity classification using a triaxial accelerometer," in *Proc. Int. Conf. IEEE Eng. Med. Biol. Soc*., vol. 3, pp. 3–5, 2003.

[41] L. Bao and S. S. Intille, "Activity Recognition from User-Annotated Acceleration Data Pervasive Computing," *Pervasive Comput.*, vol. 3001, pp. 1–17, 2004.

[42] A. H. Shultz, B. E. Lawson, and M. Goldfarb, "Running with a powered knee and ankle prosthesis," *IEEE Trans. Neural Syst. Rehabil. Eng.*, vol. 23, no. 3, pp. 403–412, 2015.

[43] J. Jang, K. Kim, J. Lee, B. Lim, and Y. Shim, "Online gait task recognition algorithm for hip exoskeleton," in *Proc. IEEE/RSJ Int. Conf. Intell. Robot. Syst. (IROS)*, pp. 5327–5332, Dec, 2015.

[44] N. Karavas, J. Kim, I. Galiana, Y. Ding, A. Couture, D. Wagner, A. Eckert-Erdheim, and C. Walsh, "Autonomous Soft Exosuit for Hip Extension Assistance," in *Proc. International Symposium on Wearable Robotics (WeRob)*, 2016.

[45] M. Tanigawa, H. Luinge, L. Schipper, and P. Slycke, "Drift-free dynamic height sensor using MEMS IMU aided by MEMS pressure sensor," in *Proc. 5th Workshop on Positioning, Navigation and Communication* (*WPNC*), pp. 191-196, 2008.

[46] P. Malcolm, F. A. Panizzolo, J. Speeckaert, J. Kim, H. Su, G. Lee, I. Galiana, K. G. Holt, and C. J. Walsh, "Effect of slope and speed on kinetics of jogging with a backpack," in *Proc. 41st Annual Meeting of the American Society of Biomechanics (ASB)*, 2017.

[47] J. M. Brockway, "Derivation of formulae used to calculate energy expenditure in man," *Hum. Nutr. Clin. Nutr.*, vol. 41, no. 6, pp. 463–471, 1987.

[48] J. R. Koller, D. H. Gates, D. P. Ferris, and C. D. Remy, "'Body-in-the-Loop' Optimization of Assistive Robotic Devices: A Validation Study," *Robot. Sci. Syst.*, Jun, 2016.

[49] J. Zhang, P. Fiers, K. A. Witte, R. W. Jackson, K. L. Poggensee, C. G. Atkeson, S. H. Collins, "Human-in-the-loop optimization of exoskeleton assistance during walking," *Science*, vol. 356, no. 6344, pp. 1280-1284, 2017.

[50] Y. Ding, M. Kim, C. Siviy, S. Kuindersma, and C. Walsh, "Human-in-the-loop multi-dimensional Bayesian optimization for hip extension assistance with a tethered soft exosuit," *Sci. Robot.,* vol. 3, no. 15, 2018.